Experimental validation of a characterization procedure for anisotropic materials using ultrasonic wave propagation techniques

Michel Darmon, Benoit Mascaro, Déborah Elbaz, Nicolas Leymarie, Philippe Guy, Sylvain Chatillon

▶ **To cite this version:**

Michel Darmon, Benoit Mascaro, Déborah Elbaz, Nicolas Leymarie, Philippe Guy, et al.. Experimental validation of a characterization procedure for anisotropic materials using ultrasonic wave propagation techniques. 2019 International Congress on Ultrasonics, Oct 2019, Bruges, Belgium. hal-02317016

HAL Id: hal-02317016
https://hal.science/hal-02317016

Submitted on 20 Oct 2023

HAL is a multi-disciplinary open access archive for the deposit and dissemination of scientific research documents, whether they are published or not. The documents may come from teaching and research institutions in France or abroad, or from public or private research centers.

L'archive ouverte pluridisciplinaire **HAL**, est destinée au dépôt et à la diffusion de documents scientifiques de niveau recherche, publiés ou non, émanant des établissements d'enseignement et de recherche français ou étrangers, des laboratoires publics ou privés.

Smart Numerical Tools for the Modelling of Ultrasonic Testing on Curved Composite Structures

Alexandre Imperiale, Edouard Demaldent, Nicolas Leymarie,
Sylvain Chatillon and Pierre Calmon

NDE department CEA LIST, Saclay, France
Corresponding author: alexandre.imperiale@cea.fr

Abstract. This communication presents a numerical computation strategy for the modelling of the ultrasonic inspections of CFRP composite structures based on a specific use of high order spectral finite elements. The overall computation performances are enhanced by considering a block-structured domain decomposition approach. This decomposition incorporates within the finite element computations relevant physical information, such as the representation of the specimen prior to and after its potential deformations, leading to an efficient reconstruction of local fiber orientations. The numerical solver is embedded within the CIVA simulation platform, and we propose several numerical illustrations of relevant 2D configurations of curved CFRP composites including potential flaws such as ply waviness.

MOTIVATIONS

Modelling high-frequency wave propagation is a major asset in ultrasonic Non Destructive Testing (NDT) as in numerous advanced industrial fields. Providing a numerical solution to these problems regroups two main challenges. First, it leads to complex and time-consuming calculation procedures. Secondly, the adequate tuning of the various numerical inputs is an intricate task, especially when the user-interface of the numerical software at hand is not dedicated to the targeted control configuration. This task is even more critical in the presence of a curved Carbon Fiber Reinforced Polymer (CFRP) composite structure such as shown in figure 1. In this context, traditional homogenization procedures lead to stratified isotropic transverse material properties [1], [2], whose anisotropic orientations depend on both the position of the layer in the stacking and the geometric deformation of the specimen (e.g. from a flat to a curved media). From a computational point of view, we must be able to define the desired local orientation at each point inside the mesh, which needs to be sufficiently fine to account for the stack in the curvature. For these practical reasons an over-refined mesh, for which the local orientation is considered to be constant in each small cell of the mesh or linearly varying between vertices, is often favored. As an example, the schematic of the grid associated with a Finite Difference Time Domain (FDTD) solution such as proposed in [3] is illustrated in figure 2 (on the right) for a straight but oblique orientation of the fibers. Layers are therefore not aligned with the cells, thus requiring a fine grid to properly model the laminate. In practice, the presence of a ply waviness such as shown in figure 2 (on the left) and, more generally, of a localized distortion of the laminate, requires to over-refine the calculation grid. Similarly, modelling intermediate layers of epoxy (isotropic medium, 10 to 25 μm thick) between homogenized carbon layers (transverse isotropic medium, 100 to 500 μm thick) penalizes furthermore the discretization. It results in a drastically limitation of the computational performance, thus making it difficult to access 3D modelling or any parametric study based on simulation.

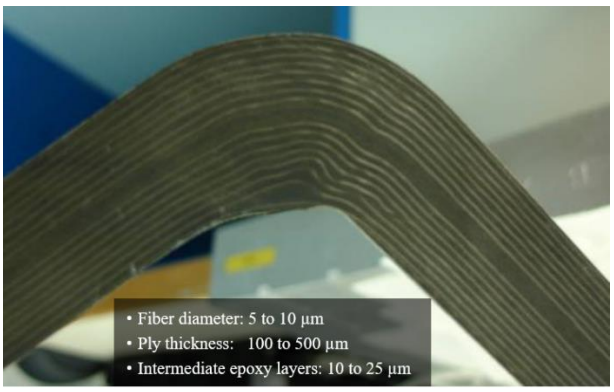

FIGURE 1. Targeted configuration of a curved stacking sequence of a CFRP laminate.

CEA LIST develops alternative modelling solutions that are meant to be use by NDT practitioners on a standard Personal Computer (PC) through the CIVA software platform. In this platform are already proposed the hybridization of a ray tracing model (to propagate the source field in the fluid between the emitter and the composite) with a 2D FDTD solution (to propagate the field inside the stacking) [3] and a ray tracing solution with full homogenization of the laminate [4]. The latter approach is satisfactory to model the ultrasonic wave in a stack of regular curvature. However, the UT signal perturbation due to a localized ply waviness is not accurately reproduced and the structural noise generated by intermediate epoxy layers with high frequency inspections cannot be adequately represented. On the other hand, the FDTD solution, even accelerated by its hybridization with ray tracing, suffers from the difficulties stated above in a distorted laminate. In order to circumvent these limitations, we propose a complementary solution, which is inspired by the previous ones. First, it is based on a hybrid approach between ray tracing in the fluid and a numerical model in the solid (coated with a thin layer of fluid). Second, the continuity of the curvature (and thus of the description of the elastic properties within each layer) as well as the regularity of the laminate before deformation are both exploited to accelerate (or more exactly to lighten) the simulation. This simulation, carried out in the time domain, is based on the use of the spectral finite element method (SEM) [5], [6] together with a specific domain decomposition method that is here adapted to the modelling of curved laminates.

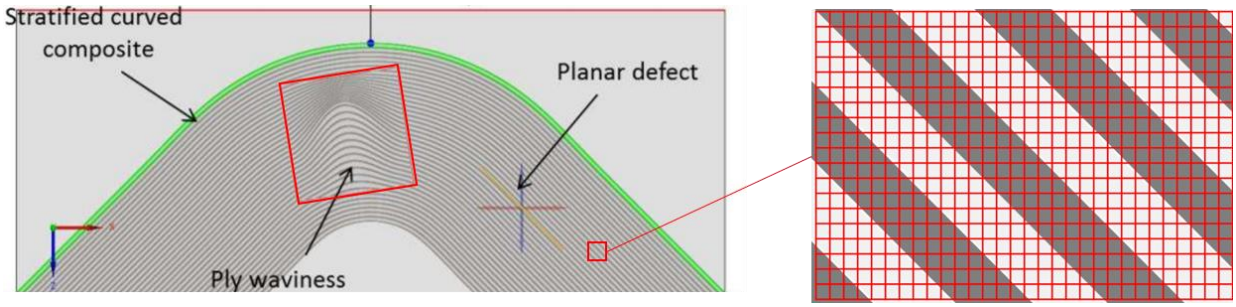

FIGURE 2. A 2D configuration of interest with ply waviness (left) [3] and an illustration of the associated FDTD grid (right)

In what follows, we present the proposed numerical strategy (a more detailed paper is in preparation). We first give the basic principles of the SEM and the domain decomposition method. We then introduce the main steps of the modelling of a curved laminated medium of CFRP type, and propose some numerical examples, here restricted to 2D simulation for bulk wave propagation, before concluding. Most of the proposed numerical tools are common to the modelling of guided (simulated in 3D, figure 3 on the left) [7] and bulk (simulated in 2D as in 3D, figure 3 on the right) wave propagation.

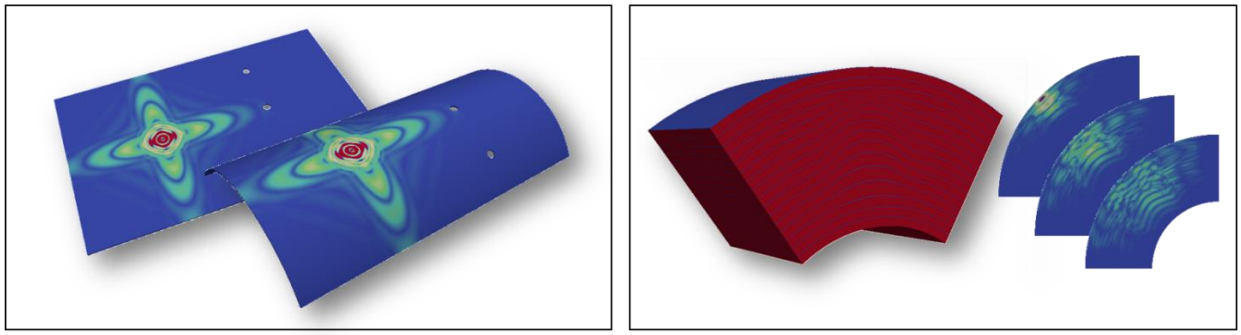

FIGURE 3. Simulation of guided (left) and bulk (right) wave propagation in curved stratified composites.

SMART NUMERICAL TOOLS ON CURVED COMPOSITE STRUCTURES

An important part of the modelling work performed at CEA LIST is focused on proposing a numerical computation strategy based on a specific use of high order spectral finite elements [8]. The overall computation performances are enhanced by considering a block-structured domain decomposition approach, denoted as the macro-element (or macro-mesh) strategy. Here we recall this strategy and extend it to the ultrasonic inspections of CFRP composite structures, where two coordinate systems representing the specimen prior to and after its deformation are considered, enabling efficient on the fly reconstruction of local fiber orientation.

Basics of the spectral finite element method

The SEM is based on a higher order Lagrange interpolation approach whose efficiency follows from the choice of the Degrees of Freedom (DoFs) at the Gauss-Lobatto quadrature points on a tensor reference element (the unit segment, quadrilateral and hexahedron in 1D, 2D and 3D, respectively, as illustrated in figure 4). This choice, together with an indexation of the DoFs on the mesh that enforces H^1 conformity of the simulated field, ensures the convergence of the numerical approximation towards the exact solution as the order of approximation increases. Moreover it leads to, first, a diagonalization of the mass matrix and, second, a factorization of the stiffness matrix. At each time step of a leapfrog time scheme, the calculation is explicit (since the inverse of the mass matrix is trivial) and the stiffness term is not stored but reassembled on the fly in the matrix-vector product that is accelerated thanks to the factorization. These properties are extensively discussed and analyzed in the literature [5]. Here we just point out the fact that the stiffness term carries the elastic properties of the medium and the local orientation of the anisotropy in a curved CFRP. Hence, if one is able to explicitly formulate the orientation of the anisotropy in the computational domain, there is no need to store the elastic properties of the medium over the complete mesh during the calculation with the SEM.

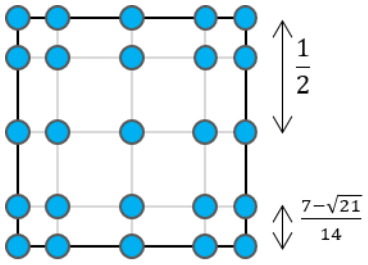

FIGURE 4. 4th order Gauss-Lobatto points on the unit quadrilateral.

Macro-mesh strategy

We propose a numerical computation strategy based on block-structured subdomains. A coarse but possibly curved (macro-) mesh carries both geometrical and physical inputs. Each element (subdomain) corresponds to a polynomial deformation of a reference macro-element (figure 5 on the left) and is associated to a unique formulation (fluid, solid, or absorbing layer). This idea is similar to the distortion of neighbor FDTD grids [9]. The communication between macro-elements is performed using the mortar element method [10] which may be used to link two macro-elements with different formulations, e.g. acoustic and elastodynamic formulations for fluid-structure interactions or elastodynamic and Perfectly Matched Layers (PMLs) formulations to model unbounded domains. Then a structured refinement of each macro-element ensures the accuracy of the SEM discretization with respect to the wavelength. The deformed grids (as shown figure 5 on the right) that are associated to every macro-elements are implicitly defined, thus significantly decreasing the overall memory load of the method: one gains in storage on the indexing of the DoFs as well as on the coordinates of the nodes in the final mesh. However, these coordinates should be stored as long as memory requirements remain acceptable for processor time efficiency. Furthermore an optimal coloring of the grid elements is used to perform unassembled finite element operations in parallel [11]. The aim of this strategy is, as explained in the introduction, to make the code usable on a standard PC.

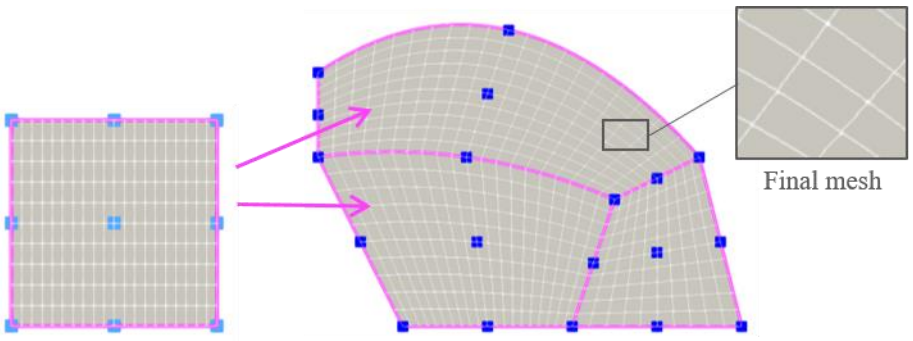

FIGURE 5. Reference macro-element with structured refinement (left) and macro-mesh with the final (distorted) block-structured mesh (right).

Meshing patterns

In our approach, since we aim at providing turnkey numerical tools suitable for parametric studies, we restrict ourselves to parametric defects from which we can deduce specific meshing patterns. Typically, an idealized crack is assimilated to an interface between two macro-elements and is modelled by elimination of the corresponding Mortar [8]. More elaborate patterns can be provided as illustrated in figure 6 for delamination and cracking at a borehole in a composite laminate.

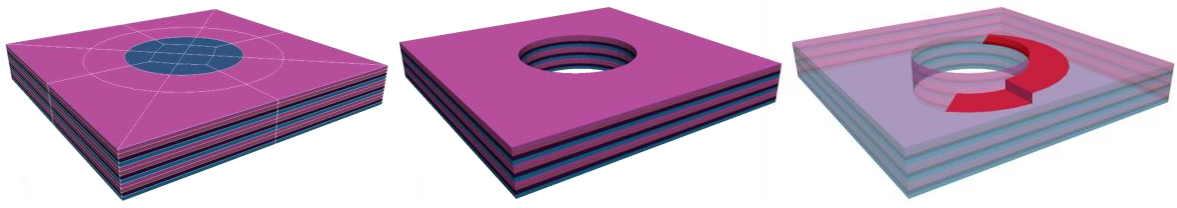

FIGURE 6. Example of macro-meshing pattern (left) whose centered macro-elements are eliminated to represent a borehole (center) and some mortar elements are eliminated to consider delamination and crack (in red on the right).

A dedicated pattern is also introduced in the presence of a sensor in contact with the SEM computational domain so that the macro-elements fit the spatial support of the source (e.g. a circle or a ring with transducers used for guided waves generation). Indeed, in the context of high order polynomial approximation, any other representation of the corresponding source terms may lead to spurious high frequency noise that would pollute the simulated signal. In the presence of several patterns, it is necessary to complete the macro-mesh. This is illustrated in figure 7 on a plane configuration viewed from above (2D mesh) with two lines of four piezo sensors and three delaminations (the red and dark blue circles in the blue boxes, respectively).

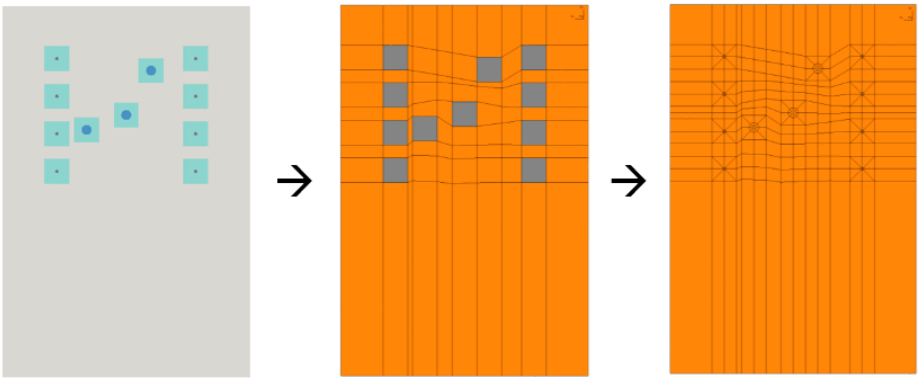

FIGURE 7. Example of the completion of a macro-mesh in presence of several patterns.

Curved stratified medium

In most of our configurations of interest, the 3D mesh is obtained by extruding a 2D mesh (such as the one in figure 7 for example) and each macro-element contains the (1D) information about the entire stratification (note that two layers of macro-elements are considered exclusively when a delamination between two plies is introduced). At this stage the orientation of the anisotropy is constant per layer and the elastic properties are expressed in the base $\mathbf{e}_i^{\Theta}(z) = \mathrm{D}\Theta(z)\mathbf{e}_i$ where $\mathrm{D}\Theta$ denotes the Jacobian matrix of the rotation Θ associated with the layer (and $\mathbf{e}_i$ the canonical base in the local coordinate system x, y, z), as illustrated figure 8, from the left to the center. In presence of a curvature, the equivalent flat scene is built then distorted according to a mapping that is read Φ on figure 8, from the center to the right. The orientation of the fibers, and therefore the elastic properties of the medium, are now expressed in the base $\mathbf{e}_i^{\Theta}(z) = \mathrm{D}\Phi(x, y, z)\,\mathrm{D}\Theta(z)\mathbf{e}_i$ where $\mathrm{D}\Phi$ denotes the normalized Jacobian matrix of the mapping Φ. This normalization is a modelling choice to ensure that only the direction of anisotropy varies, not its amplitude. In particular, an isotropic medium remains isotropic after deformation. Finally, a ply waviness, as the one illustrated in figure 2, is given by combining the global deformation Φ with a local one.

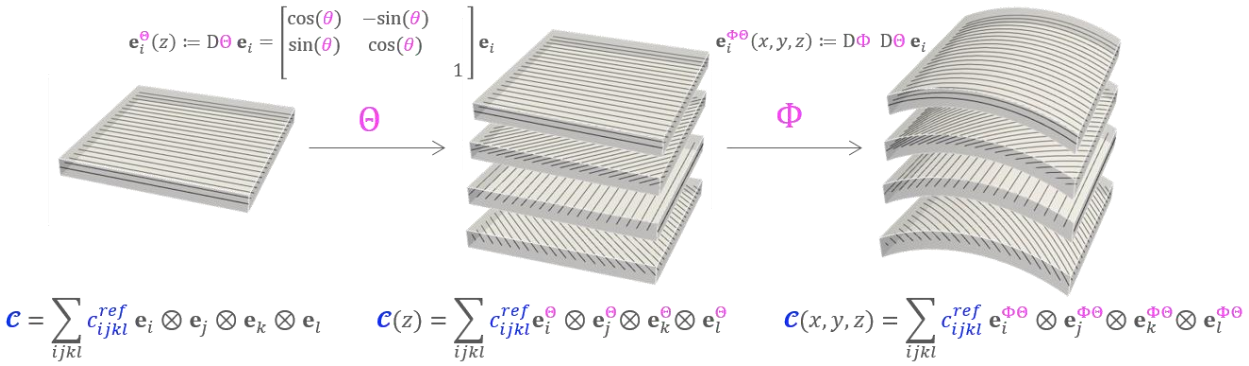

FIGURE 8. Formulation of the elastic properties with respect to a reference layer and a mapping.

From an implementation point of view, we store the two sets of coordinates of the nodes of the macro-mesh, prior to and after its deformation, to synthesize the mapping Φ. This causes no difficulty in memory requirements since the macro mesh is (very) coarse. Passing from one system to the other enables efficient on the fly reconstruction of local fiber orientation in $\boldsymbol{\mathcal{C}}(x, y, z)$ and therefore efficient stiffness matrix-vector product within the SEM applied to the refined mesh. The refinement of the macro-mesh is set to match the stacking: each cell of the final mesh belongs only a single layer of the laminate. Finite elements of anisotropic order are used to reduce the order of approximation within the thickness in thin layers so as not to penalize spatial as well as time discretization. PMLs are designed on the flat geometry with a reverse deformation (Φ^{-1}) to ensure stability even in curved domains.

APPLICATION TO THE SIMULATION OF UT INSPECTIONS ON CFRP

Test case description

We are currently working on the introduction of these models in the CIVA platform. The composite module GUI has been preserved (in common with FIDEL and ray tracing solutions). Here we propose a testing configuration in a curved specimen with ply waviness. The curvature radius is about 20 mm and the thickness of the plate is equal to 7.23 mm. The stratified structure consists of 14 repetitions of pairs of [0°/90°] oriented layers of 244 µm thickness with intermediate epoxy layers of 15 µm thickness (for a total of 2×14 + 27 = 55 layers). Each ply is considered as a transversely isotropic material where the symmetry direction corresponds to the fiber alignment axis. The material properties are given in table 1.

TABLE 1. Material properties of CFRP components (density and stiffness matrix) used for all simulations.

	Density	**Stiffness matrix components (GPa)**								
	(g.cm^{-3})	C_{11}	C_{22}	C_{33}	C_{12}	C_{13}	C_{23}	C_{44}	C_{55}	C_{66}
Ply	1.6	143.2	15.8	15.8	7.5	7.5	8.2	3.8	7	7
Epoxy	1.23	7.6	7.6	7.6	4.4	4.4	4.4	1.6	1.6	1.6

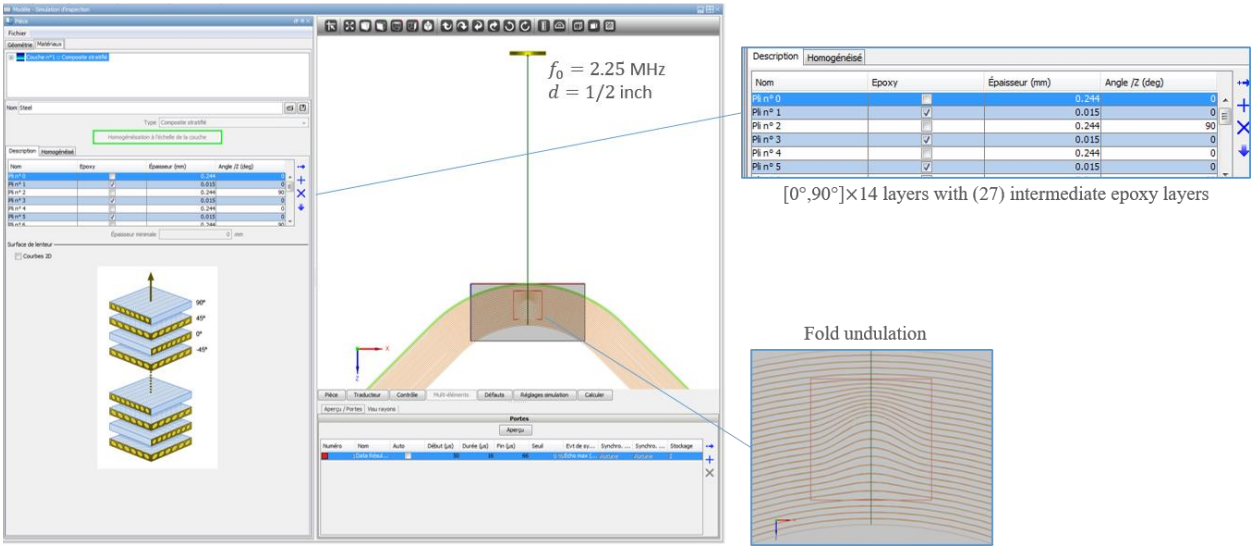

FIGURE 9. Nominal test case definition and its representation in CIVA GUI.

The composite structure is considered to be completely immersed in water. The source is a circular transducer with a ½-inch diameter whose center frequency is, unless otherwise stated, 2.25 MHz. The probe is always placed 40 mm above the laminate surface as shown in figure 9. In this figure, note that each line does not correspond to the boundary between two layers but to an intermediate epoxy layer of 15 µm (which is meshed).

SEM calculation

The SEM as well as the hybridization with ray tracing algorithms are automatically configured. As for the FIDEL module in CIVA, the incoming field in fluid is calculated by ray tracing and reciprocity is performed in the fluid, at the interface with the absorbing layer. Mortar elements handle the fluid-solid coupling as well as the coupling with the (possibly curved) PMLs. Some snapshots of the field solution are shown in figure 10 where the various subdomains are labelled.

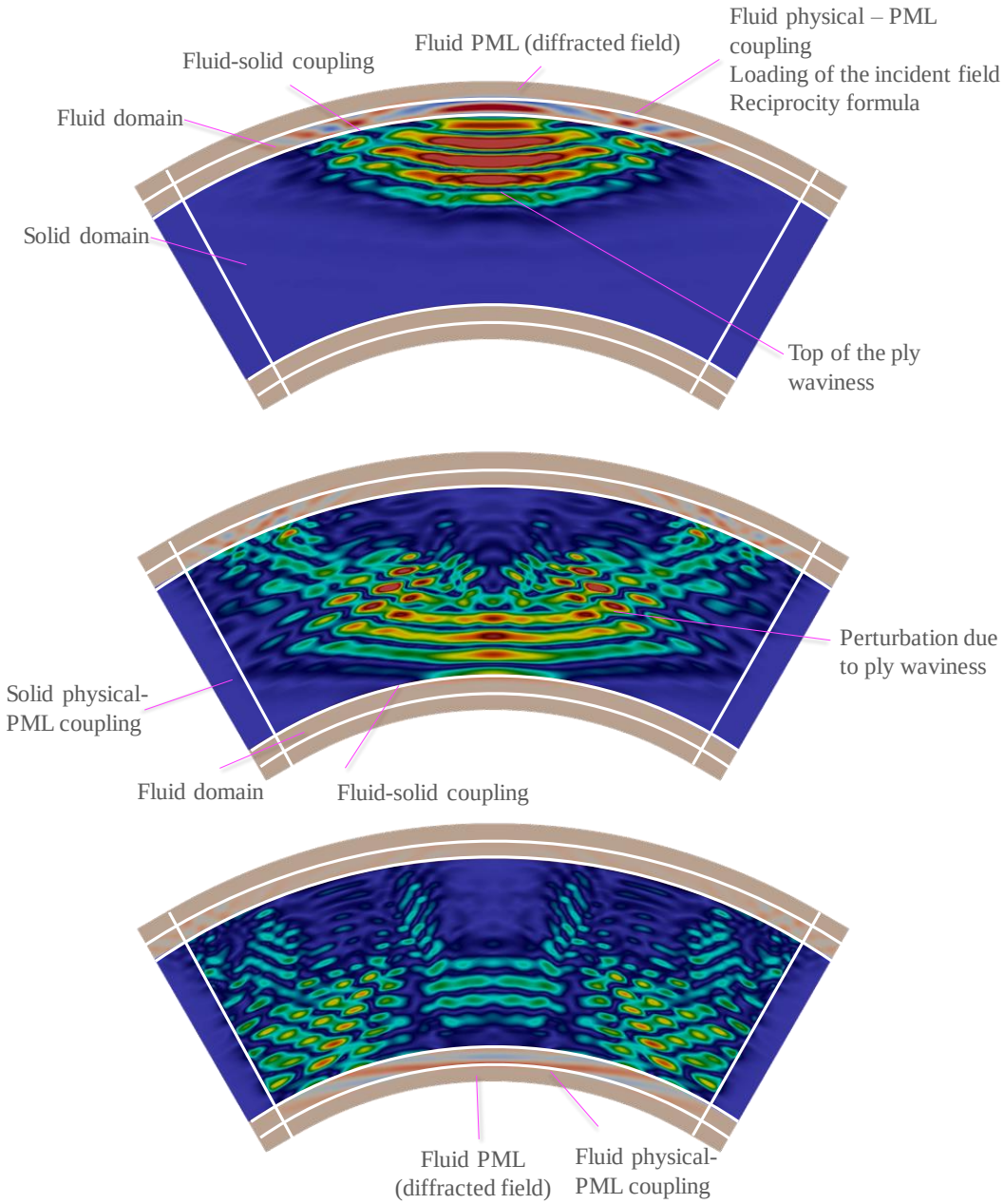

FIGURE 10. Snapshots of the SEM solution. In white lines are the edges of the macro-elements. The color corresponds to the magnitude of the displacement field (solid subdomains) or the pressure field (fluid subdomains).

Results

Figure 11 shows the AScan echo responses from 50 to 66 µs (2 back and forth) with and without considering ply waviness. The healthy signal is simulated in less than a minute and the one with the ply waviness in 2 minutes (all presented CPU times were obtained with an Intel® core™ i7-6820mq CPU 2.70 GHz). The number of unknowns is identical from one simulation to another. The gap in computation time is due to the increase in the number of time steps in presence of the ply waviness (we recall that the time step behaves like the ratio of the smallest edge of the mesh on the largest).

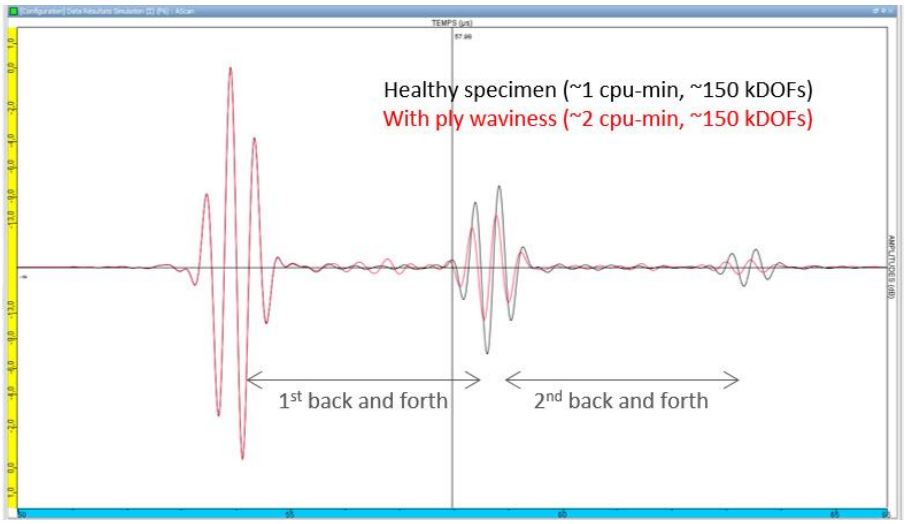

FIGURE 11. A-scan signals of the healthy specimen (in black) and with ply waviness (in red).

These low computation times make the generation of realistic B-scan images, such as the one presented in figure 12, tractable. By comparing both images, we observe that the ply waviness generates only few backscattering and is therefore not visible in the anomaly area. However, its signature comes from its indirect effect characterized by a local amplitude loss of the backwall echo.

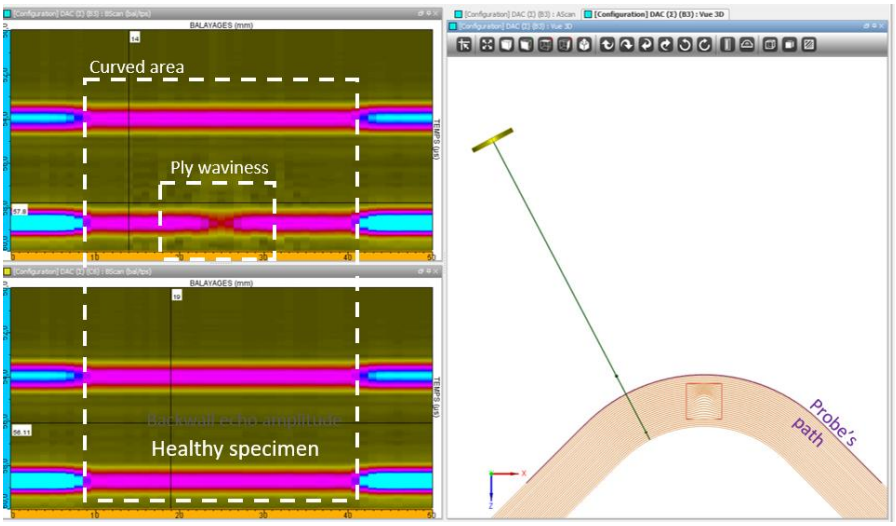

FIGURE 12. B-scan images of the healthy specimen (bottom left) and with ply waviness (top left, right) using a surface echo signal equalization by DAC (Depth Amplitude Compensation) function.

In the presented results, the anisotropic attenuation phenomena, such as observed in composite materials, are not accounted for in the finite element model. Similarly to [12], attenuation is taken into account as a post-processing of the UT signal performed without attenuation. The A-scan filtering operation is applied as a time sliding window using various damping frequency filters with respect to the depth of propagation on the focal axis inside the sample. An illustration of the effect of the attenuation on the received signal is shown in figure 13.

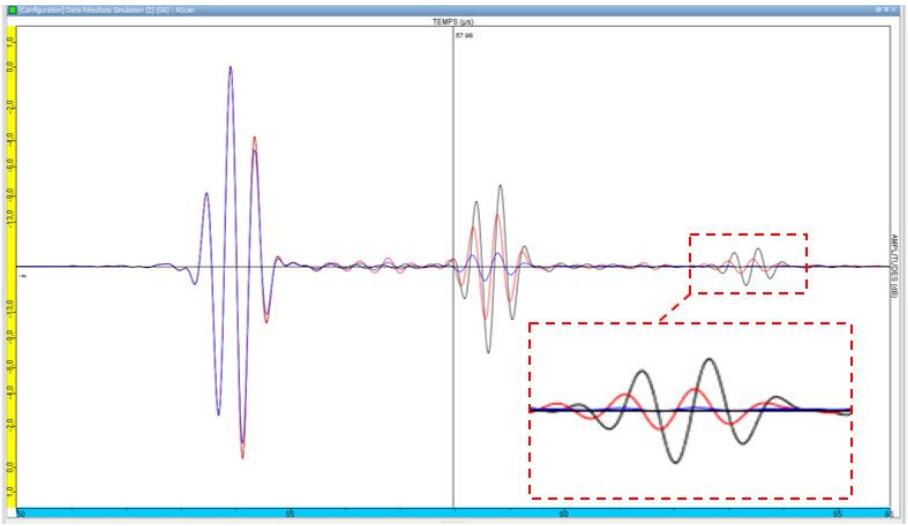

FIGURE 13. A-scan signals of the healthy specimen (in black) and with ply waviness, with (in blue) and without (in red) attenuation.

In a last simulation, the center frequency f_0 of the probe has been shifted to 6 MHz in order to observe specific structural noise due to the presence of intermediate epoxy layers in such laminate. As shown in figure 14, this phenomenon is well reproduced in the FE solution.

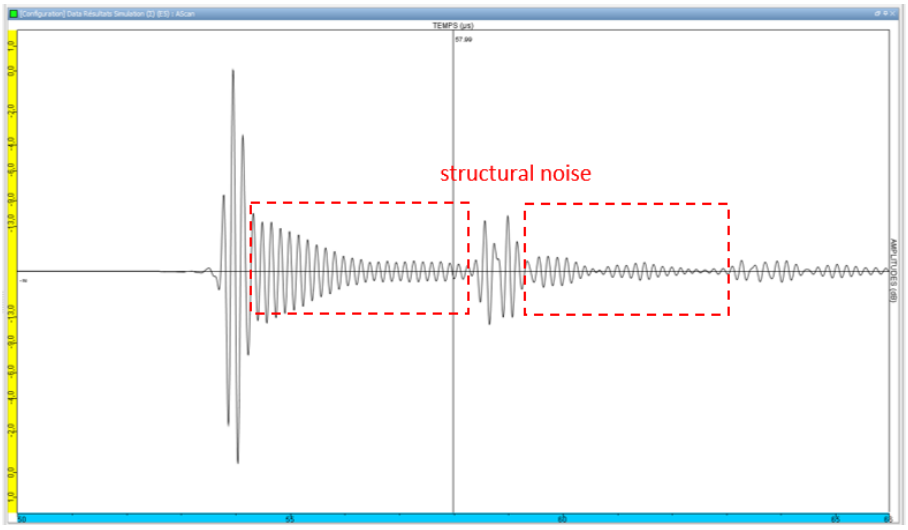

FIGURE 14. A-scan signals of the healthy specimen changing the center frequency f_0 = 6 MHz so that structural noise in such laminate can be observed in this frequency bandwidth.

PERSPECTIVES

In all the simulations presented in the previous section, the cost in memory did not exceed 100 or 200 MB, which augurs well for achieving a functional 3D solution on a standard PC. The SEM for 3D laminated structures with ply waviness is already operational (see for example the test case presented in [12]) and its integration in CIVA is in progress. It remains in particular to modify the implementation of the reciprocity formula to preserve reasonable memory loads as the convolution is performed on wide temporal and spatial domains in comparison with the previous SEM applications already available in CIVA [13]. Beyond developments, the next challenge will be to experimentally confirm the relevance of the proposed model in a curved composite. Besides, the modeling strategy presented in this contribution is already exploited in 3D to simulate guided wave propagation for modelling structural health monitoring (SHM) applications [14], and a specific module is under development.

REFERENCES

[1] S. Lonné, A. Lhémery, P. Calmon, S. Biwa, and F. Thévenot, "Modeling of Ultrasonic Attenuation in Uni-Directional Fiber Reinforced Composites Combining Multiple-Scattering and Viscoelastic Losses," in *AIP Conference Proceedings*, 2004, vol. 700, pp. 875–882.

[2] S. Deydier, N. Leymarie, P. Calmon, and V. Mengeling, "Modeling of the Ultrasonic Propagation into Carbon-Fiber-Reinforced Epoxy Composites, Using a Ray Theory Based Homogenization Method," in *AIP Conference Proceedings*, 2006, vol. 820, pp. 972–978.

[3] F. Reverdy, S. Mahaut, N. Dominguez, and P. Dubois, "Simulation of ultrasonic inspection of curved composites using a hybrid semi-analytical/numerical code," in *AIP Conference Proceedings*, 2015, vol. 1650, pp. 1047–1055.

[4] S. Journiac, N. Leymarie, N. Dominguez, and C. Potel, "Simulation of ultrasonic inspection of composite using bulk waves: Application to curved components," in *Journal of Physics: Conference Series*, 2011, vol. 269, p. 012022.

[5] G. Cohen, *Higher-Order Numerical Methods for Transient Wave Equations*. Berlin Heidelberg: Springer-Verlag, 2002.

[6] D. Komatitsch and J. Tromp, "Introduction to the spectral element method for three-dimensional seismic wave propagation," *Geophys J Int*, vol. 139, no. 3, pp. 806–822, Dec. 1999.

[7] O. Mesnil, A. Imperiale, E. Demaldent, V. Baronian, and B. Chapuis, "Simulation tools for guided wave based structural health monitoring," in *AIP Conference Proceedings*, 2018, vol. 1949, p. 050001.

[8] A. Imperiale, S. Chatillon, P. Calmon, N. Leymarie, S. Imperiale, and E. Demaldent, "UT simulation of embedded parametric defects using a hybrid model based upon spectral finite element and domain decomposition methods," in *19th World Conference on Non-Destructive Testing*, 2016, vol. 1, pp. 2184–2189.

[9] L. Dovgilovich and I. Sofronov, "High-accuracy finite-difference schemes for solving elastodynamic problems in curvilinear coordinates within multiblock approach," *Applied Numerical Mathematics*, vol. 93, pp. 176–194, Jul. 2015.

[10] F. B. Belgacem, "The Mortar finite element method with Lagrange multipliers," *Numer. Math.*, vol. 84, no. 2, pp. 173–197, Dec. 1999.

[11] C. Carrascal-Manzanares, A. Imperiale, G. Rougeron, V. Bergeaud, and L. Lacassagne, "A fast implementation of a spectral finite elements method on CPU and GPU applied to ultrasound propagation," in *International Conference on Parallel Computing*, Bologna, Italy, 2017, vol. 32, pp. 339–348.

[12] K. Jezzine, D. Ségur, R. Ecault, N. Dominguez, and P. Calmon, "Hybrid ray-FDTD model for the simulation of the ultrasonic inspection of CFRP parts," in *AIP Conference Proceedings*, 2017, vol. 1806, p. 090016.

[13] A. Imperiale, N. Leymarie, E. Demaldent, and T. Fortuna, "Coupling strategies between asymptotic and numerical models with application to ultrasonic non-destructive testing of surface flaws," *Journal of Theoretical and Computational Acoustics*, accepted for publication.

[14] O. Mesnil, A. Imperiale, E. Demaldent, and B. Chapuis, "Validation of Spectral Finite Element Simulation Tools Dedicated to Guided Wave Based Structure Health Monitoring," in *AIP Conference Proceedings, QNDE 2018*.